Nanoscale

Accepted Manuscript

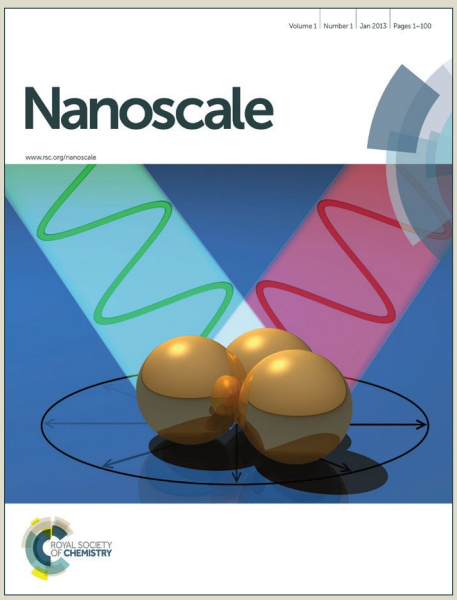

ROYAL SOCIETY OF CHEMISTRY

www.rsc.org/nanoscale

Nanoscale

ARTICLE

In vitro Cardiomyocytes-Driven Biogenerator Based on Aligned Piezoelectric Nanofibers

Received 00th January 20xx,
Accepted 00th January 20xx

DOI: 10.1039/x0xx00000x

www.rsc.org/

Xia Liu,[a,b] Hui Zhao,[c] Yingxian Lu,[a,b] Song Li,[d] Liwei Lin,[e] Yanan Du[c] and Xiaohong Wang[a,b,*]

Capturing body's mechanical energy from the heart, lung, and diaphragm can probably meet the requirements for *in vivo* applications of implantable biomedical devices. In this work, we present a novel contractile cardiomyocytes (CMs) driven biogenerator based on piezoelectric nanofibers (NFs) uniaxially aligned on a PDMS thin film. Flexible nanostructures interact with CMs, as physical cue to guide the CMs to align specifically, and create mechanical interfaces of contractile CMs and piezoelectric NFs. As such, the cellular construct is featured by specific alignment and synchronous contraction, which realizes the maximal resultant force to drive the NFs to bend periodically. Studies on contraction mapping display that neonatal rat CMs self-assemble into a functional bio-bot film with well-defined axes of force generation. Consequently, the biogenerator produces an average voltage of 200 mV and current of 45 nA at the cell concentration of 1.0 million/ml, offering a biocompatible and scalable platform for biological energy conversion.

Introduction

Converting energy in the human body into electricity can provide a lifetime power source, applied in various wearable electronics and potentially implanted microdevices.[1,2] On the one hand, capturing the mechanical energy from our personal activities like walking, typing, and breathing, enables to drive personal electronics. On the other hand, making use of *in vivo* mechanical, biochemical or possibly electromagnetic energy is a straightforward way to power implantable microdevices. Piezoelectric thin films can convert ambient mechanical energy into electric signals, even responding to tiny movements on corrugated surfaces of internal organs, such as inhaling/exhaling of lungs or heartbeat.[3,4] Dagdeviren et al. proposed a flexible PZT mechanical energy harvester that was mounted on the right ventricle of a bovine heart and yielded significant electrical power from movements of the heart.[4] More attractively, contractile cells act as the engine of the heart motion, such as CMs featuring the sophisticated self-contraction actuation and the potential in biomechanical energy conversion.[5,6] CM-inspired actuation systems perform functions as diverse as gripping, walking, and swimming with fine spatial and temporal control, such as 2D biohybrid muscular thin films,[5,7] walking biological machines,[2,8,9] and swimming engineered jellyfishes.[10] These engineered constructs are spatially ordered and most specifically micropatterned by micro contact printing method. Functionalizing CMs-actuated systems with piezoelectric mode is an excellent route to convert biomechanical energy to electricity. Ishisaka et al. demonstrated a single lead zirconate titanate (PZT) fiber generator driven by a bunch of CMs randomly distributed on a PDMS membrane.[11,12] While, Choi et al. achieved irregular electricity output converted from the biomechanical energy of CMs which self-organized directly on a piezoelectric lead magnesium niobate–lead titanate (PMN–PT) diaphragm with the result of irregular output voltage.[13] Therefore, we tried to uniaxially align the CMs on a piezoelectric polyvinylidenefluoride (PVDF) thin film to convert their contraction energy to a periodic electric output.[14]

[a] Institute of Microelectronics, Tsinghua University, Beijing 100084, PR China. E-mail: wxh-ime@tsinghua.edu.cn; Tel: +86-010-62798432
[b] Tsinghua National Laboratory for Information Science and Technology, Tsinghua University, Beijing 100084, PR China
[c] Department of Biomedical Engineering, School of Medicine, Collaborative Innovation Center for Diagnosis and Treatment of Infectious Disease, Tsinghua University, Beijing 100084, PR China
[d] Department of Bioengineering, University of California, Berkeley 94720, USA
[e] Department of Mechanical Engineering, University of California, Berkeley 94720, USA
†Electronic Supplementary Information (ESI) available.
See DOI: 10.1039/x0xx00000x

The efficiency of converting contraction energy of CMs into electricity relies on cell alignment and the transducing microstructure. The uniaxial alignment of the myocardial cell sheet efficiently add up the contraction forces of all the CMs,[4,5] compared with actuation movement of randomly distributed CMs.[11-13] The piezoelectrics with microstructures (e.g. PZT fibers,[11,12] PVDF films,[14] ZnO nanowires,[15] and PVDF NFs[16]) can be used to exploit deformations induced by nano scaled forces, like ultrasonic waves, pressure, tension/compression, twisting or mechanical vibration. Although PZT is a general material used for mechanical energy harvesting,[17] it is less advantageous in sustainable and environmental friendly applications due to its toxicity and non-biocompatiblility.[18] While PVDF NFs are among the best candidates featured by their one-dimensional nanostructures, favourable biocompatibility and high piezoelectric properties.[19-21]

We developed a contractile cardiomyocytes driven piezoelectric nanofiber (CCDPN) biogenerator featured by the NFs, which are easier to bend due to higher elastic coefficient and can be used as physical cue to guide the CMs to align specifically. Fig. 1 illustrates the concept of the cellular mechanical energy conversion to electricity. Flexible nanostructures interact with CMs, i.e., to create mechanical interfaces and guide the contraction direction of CMs along the long-axis direction of NFs (Fig. 1a). Cell-to-cell electromechanical coupling promotes tissue-wide propagation of electrical impulses and spatiotemporal synchronization of the contraction,[22] which differentiates CMs in Fig. 1b from most other contractile cell types, like skeletal myocytes.[23,24] As a consequence of cooperative contraction of CMs responding to the nanoscale features of the NFs in Fig. 1c, the biogenerator can bend further out of the plane. Its energy conversion efficiency depends on the consistence in the contraction direction and the electron transportation.

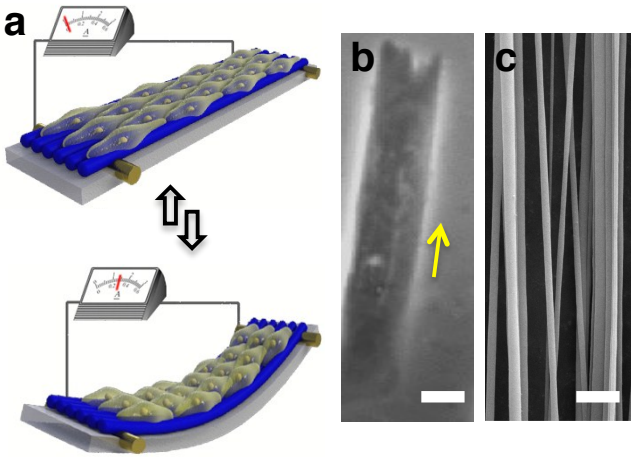

Fig. 1 (**a**) The schematic overview presents contractile cardiomyocytes driven piezoelectric nanofiber (CCDPN) biogenerator. Isolated cardiomyocytes (CMs) are cultured on a uniaxially aligned piezoelectric nanofiber (NF) mat with both ends tightly attached to the substrate and outlet interconnects. Synchronous contraction of the CMs creates a concentrated compressive strain and a corresponding piezoelectric potential in the CCDPN biogenerator, driving electrons through the external load. (**b**) Single CM contracts spontaneously in the long-axis direction (the yellow arrow). (**c**) SEM image of piezoelectric PVDF NF with uniaxial alignment. Scale bar, 20μm (b), 5μm (c).

Experimental sections

Fabrication of CCDPN biogenerators

The solution of 5 wt% poly-N-Isopropylacrylamide (PNIPAM, Sigma-Aldrich, No. 731048) in 1-butanol (w/v) was spin coated onto the glass cover slip at 3,000 RPM for 1 minute to build a thermally sensitive sacrificial layer firstly. PDMS (Sylgard 184) elastomer was mixed at 10:1 base to curing agent ratio and spin coated on top of the PNIPAM-coated cover slip at 6,000 RPM for 2 minutes. Then the PDMS film was partially solidified by curing at 60 °C for 4 hours. The curve of viscosity to time is dependent on the temperature (Fig. S1). After surface insulation process, two gold wires, as the electrodes of the CCDPN biogenerator, were manually partially embedded in the two parallel edges of the semi-cured PDMS film under an inverted microscope.

Then, to pattern NFs on the semi-cured PDMS film, specific gap collectors were designed, like a pair of parallel electrodes for uniaxial alignment and concentric ring electrode for random straight pattern (Fig. S2). Then PVDF NFs would be settled on the semi-cured PDMS film crossing the gold wires. Electrospinning technique was started with loading the solution (1.6 g PVDF powder in 4.0 ml DMAC and 6.0 ml acetone) into a 1.0 ml plastic syringe tripped with a 25-gauge stainless steel needle. The positive lead from high voltage supply was connected to the metal needle applied with the bias value around 30 kV. The solution was injected into the needle at a constant rate of 1.0 mlh^{-1} with a syringe pump. The distance was 12 cm from the needle to the designed gap collector grounded. The semi-cured PDMS film with gold wires was fixed inside the gap collector. So the as-electrospun piezoelectric PVDF NFs crossed the wires and meanwhile formed fused junctions with the biogenerator electrodes, as highlighted in the fabrication process of Fig. S3.

Nanofiber characterizations

X-ray diffraction (XRD) patterns of aligned NF mats and random NF mats were recorded using D/max2550HB+/PC diffractometer (Rigaku, Japan) with Cu (40 kV, 200 mA) Kα radiation. Fourier transform infrared spectroscopy (FTIR) can be used to characterize both the dipole orientation and crystallographic structure of NFs based on the sensitivity of CF_2 orientation changes. FTIR spectra of aligned NF mats and random NF mats were collected in attenuated total reflectance (ATR) mode using a spectrophotometer (Bruker 13006875, Germany). Samples were placed on top of the ATR set and scanned from 2,000 to 600 cm^{-1}. A total of six scans were collected for signal averaging.

Nanofiber surface functionalization

The nanofibers on the PDMS thin film were coated with fibronectin (Sigma-Aldrich, No. F0895). Immediately prior to fibronectin treatment the device constructs were oxidized using UV ozone overnight to sterilize the surfaces and increase hydrophilicity for the interaction. All subsequent processing was performed in biohood under sterile conditions. Fibronectin was deposited by placing a 1 ml droplet of 10 μg/ml fibronectin in sterile Hank's balanced salt solution (HBSS) on the device array (2cm × 2cm) and incubating for 30 minutes. Following fibronectin incubation period, excess protein was removed by washing 3 times with HBSS and then air dried prior to cell seeding.

Cell isolation and culture

Neonatal rat ventricular cardiomyocytes were isolated from two-day-old Sprague-Dawley rats. All procedures were conducted in accordance with the guidelines of the Institutional Animal Care and Use Committee (IACUC) at Tsinghua University. Firstly, ventricles were surgically isolated and homogenized by washing in HBSS followed by digestion with 0.1% trypsin overnight at 4 °C. After the supernatant discarded, the second digestion was started by adding digest enzyme (0.1% (v/v) collagenase type II in HBSS) at 37 °C water bath with stir bar for 8 minutes and then was repeated for around eight times until the ventricle tissues became tiny. Subsequently, cells were re-suspended in DMEM culture medium supplemented with 10% (v/v) heat-inactivated fetal bovine serum (FBS), and 1% (v/v) Penicillin/Streptomycin. The isolated CMs were evenly seeded at a density of 0.5 million cells (0.5 ml cell suspension with the concentration of 1 million/ml) per cover slip (2cm × 2cm) and incubated under standard conditions at 37 °C and 5% CO_2. After 24 hours incubation, the constructs were washed three times with the culture medium to remove non-adherent cells and then covered with the fresh culture medium. Every other day the medium was changed with maintenance medium.

Cellular characterizations

Environmental scanning electron microscopy

CMs cultured on NFs were fixed with 2.5% glutaraldehyde in deionized water for two hours, gently washed three times, and then dehydrated with series of graded ethanol (30, 50, 70, 80, 90 and 100%). The samples were subsequently immersed in tert-butyl alcohol twice, each for three minutes and frozen at -20 °C. Morphology of cells and NFs was visualized by a scanning electron microscope (SEM, FEI Quanta 450, Netherlands) at water environment.

Immunofluorescence staining and imaging

Samples were removed from the incubator, washed three times with PBS at 37 °C and fixed for 20 minutes in 4% paraformaldehyde and 0.5% TritonX-100 in PBS for another 20 minutes at room temperature, followed by being blocked with 5% (w/v) bovine serum albumin (BSA, Wissent, Canada). Fixation samples were stained for 1 hour at room temperature with 1:200 dilutions of mouse anti-sarcomeric α-actinin monoclonal primary antibody. Samples were then washed three times with PBS and concurrently stained with 1:200 dilutions of DAPI, phalloidin conjugated to Alexa-Fluor 488 (Invitrogen) and goat anti-rabbit conjugated to tetramethylrhodamine secondary antibodies for 1 hour at room temperature. Samples were then washed three times with PBS, mounted to glass slides and imaged on a confocal microscope (AXIOobserze.Z1, Zeiss).

AFM characterization

An AFM system (NanoWizard®, JPK Instrument, Germany) and silicon nitride microcantilevers (nominal spring coefficient 0.2 N/m; MLCT, Veeco, USA) were used. The entire setup was enclosed in a customized chamber maintained at 37 °C. The CMs typically retained stable contraction for 2 to 4 hours after removal from the incubator and placement in the chamber. All data presented here were obtained within 30 minutes. The microcantilever was brought into gentle contact with the cell. The force exerted on the cell by the microcantilever was kept constant with a feedback loop and a piezo tube that moved the cantilever vertically while the cell was beating. The temporal movement of the cell membrane was thereby tracked precisely with the displacement of the microcantilever. As described, the load exerted on the CM was maintained constant while the cell contracted. The amplitude determined under this condition accordingly represents the contractile strength or the contractility of CMs that are undergoing isotonic contraction.

Results and discussion

Physical constraint by extracellular matrix represents one of critical mechanisms for regulating self-assembly of subcellular structures.[25] The spontaneous response of synchronous contraction to the alignment pattern of myocardial cell sheets depends on the nanostructure morphology of NFs. Piezoelectric nanostructure is customized in developing fiber materials to boost anisotropy of myocardial cell sheets. The electrospun PVDF NFs were collected on a semi-cured PDMS film using specific nanofiber-collecting electrodes, in which textured structure was revealed by SEM images (Fig. 2). Having been collected using the grounded electrode pair (Fig. S2), the NFs crossed the gold wire and partially embedded into the PDMS substrate in parallel, as demonstrated in Fig. 2a. In contrast, the grounded concentric ring electrode (Fig. S2) encircling the PDMS substrate was used to collect the random NFs (Fig. 2b). We found two gold wires, as the electrodes of the CCDPN biogenerator, were sandwiched between the PDMS film and PVDF NFs. The fused junctions between the NFs and gold wires were formed, which unified the piezoelectric nanomaterials and the biogenerator electrodes, as observed in Fig. 2(a1) and 2(b1). And the as-electrospun NFs were partially embedded in the semi-cured PDMS film due to electric field force and Columbic force (Fig. 2(a2) and 2(b2)).

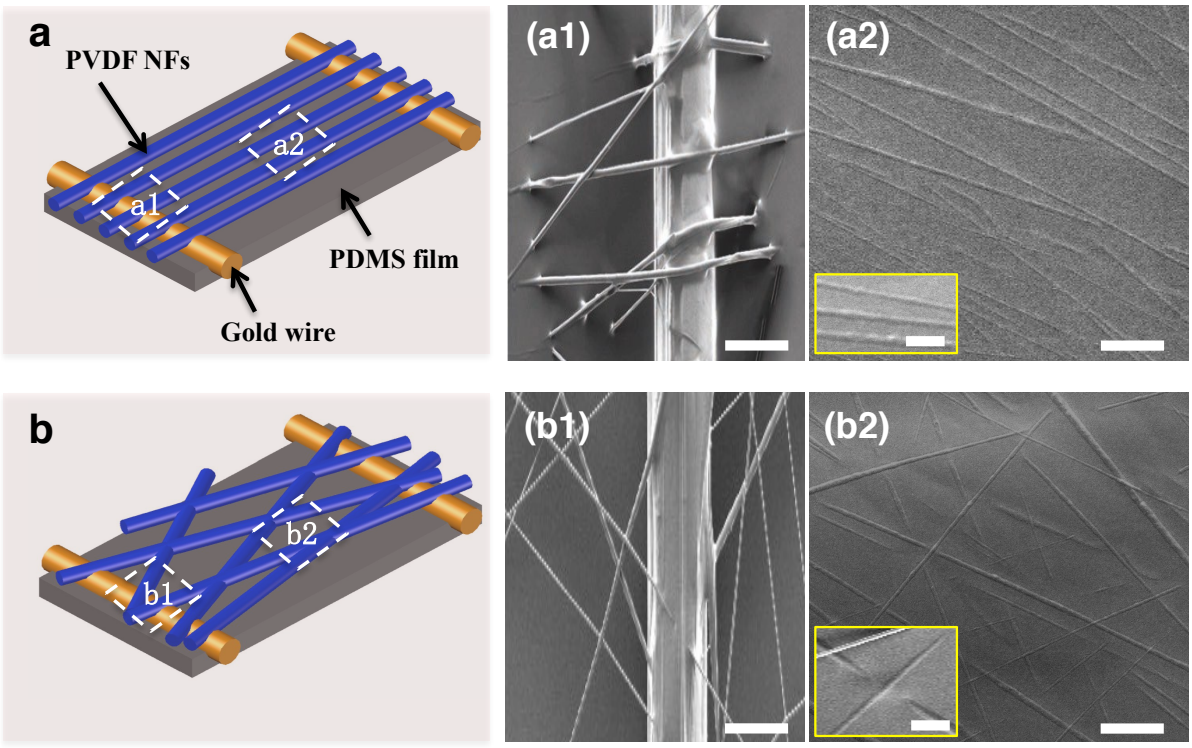

Fig. 2 (**a**) The uniaxially aligned NFs cross two gold wires that are partially embedded into the PDMS film. The section (**a1**) is demonstrated by the SEM image of the aligned NFs across the gold wire, and the section (**a2**) shows the parallel NF array that partially root in the PDMS film. (**b**) In contrast, the random NFs cross two gold wires as well. The section (**b1**) shows the random NFs cross the gold wire, and the section (**b2**) shows the NFs are randomly distributed and partially embedded in the substrate. The insets in (a2) and (b2) zoom in on the NFs that partially root in the PDMS film. (The scale bars are 10 μm except the insets are 5 um.)

Crystalline analysis is presented in Fig. 3a and 3b. Fourier transform infrared spectroscopy (FTIR) was used to characterize the crystal phases present in the PVDF NFs. A mixture of the polar β phase and the non-polar α phase was indexed. The characteristic absorption bands at 843 cm^{-1} (CH_2 rocking), 1072 cm^{-1} (C–C stretching band), 1275 cm^{-1} (trans band), and 1432 cm^{-1} (CH_2 bending) are attributed to the piezoelectric all-trans β phase (Fig. 3a). There is almost no difference between the random NF mat and the aligned NF mat. The XRD patterns of the aligned and random NF mats both showed the (110) reflection of the β phase formation with a prominent peak at 20.6° (Fig. 3b). The proportion of the β phase increased to 68.4%, when the electrospinning voltage was 30 kV. From XRD and FTIR results it can be concluded that high voltage can induce the formation of β or γ polar crystals in PVDF; therefore, the PVDF composites acquired piezoelectric properties. Then piezoelectric NF generator on a PDMS thin film driven by motors can yield open-circuit voltage of 0.6 V_{pp} for the aligned pattern and 0.02 V_{pp} for the random pattern, as presented in Fig. 3c and 3d, respectively.

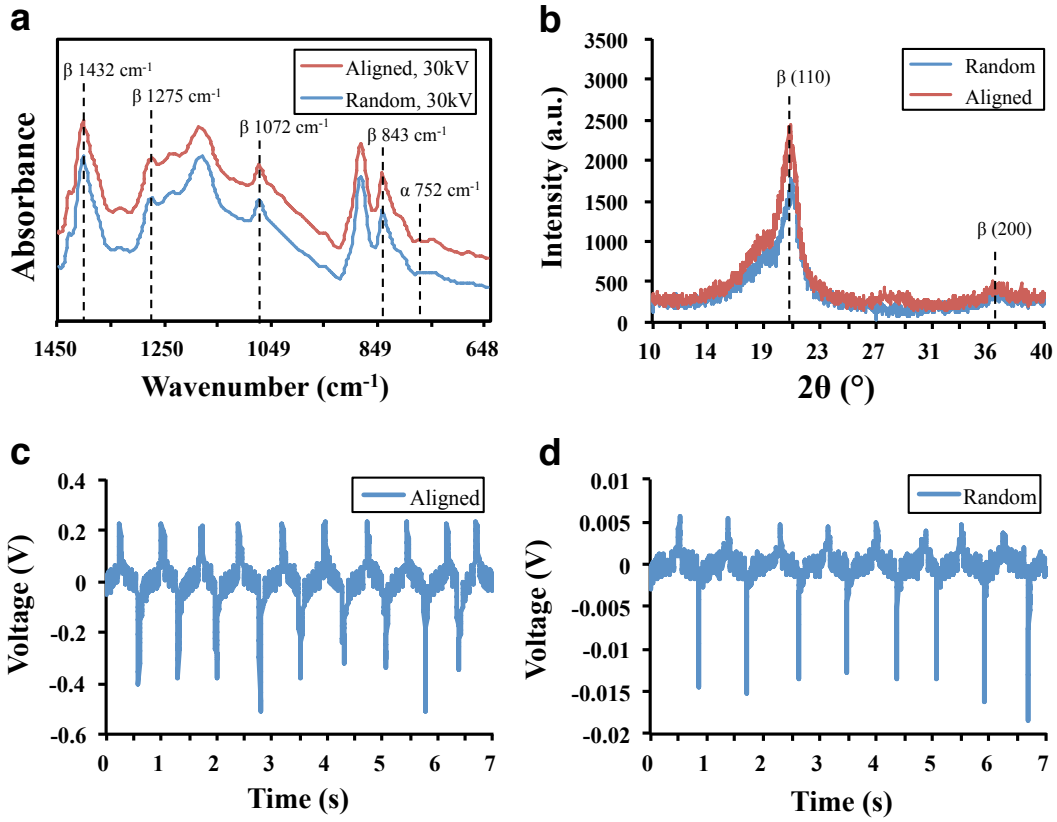

Fig. 3 (**a**) The FTIR spectra in the ATR mode for aligned NFs and random NFs. (**b**) The XRD pattern of the as-electrospun piezoelectric PVDF NFs shows the polar phases β (110) and β (200). The open-circuit voltage of (**c**) the piezoelectric aligned NF generator and (**d**) the piezoelectric random NF generator corresponding to the bending state and the release state.

We engineered anisotropic and isotropic cell sheets on fibronectin-coated PVDF NFs by passively seeding dissociated ventricular CMs. Fibronectin forming chemical bonds with PVDF chains acts as the interfacing chemistry to elicit cell adhesion and growth. Therefore, intrinsic functionality of CMs is maintained through mechanical interfaces between contractile CMs and piezoelectric NFs. Indeed, anisotropic cell sheets have uniaxial alignment of cell bodies, while isotropic cell sheets have no net alignment of cell bodies, as shown in Fig. 4a and 4e. The interface between the single CM and its attached NFs can be observed within the specimen chamber of an environmental scanning electron microscope (ESEM), which breadcrumbs in an attempt to gain insight into the structural characteristics. The long axis of the CMs on the uniaxially aligned NF mat is parallel to the orientation of NFs (Fig. 4b), while the CM on the random NF mat has a pentagon shape (Fig. 4f). Stainings for sarcomeric α-actinin (red), F-actin (green) and nuclei (blue) reveal uniaxial sarcomere alignment for aligned pattern (Fig. 4c, Fig. S4); in contrast to, no preferential alignment of sarcomeres along any axis for random pattern (Fig. 4g, Fig. S4).[26] Aligned proportion here was defined as percentage of the 90°±10° angle between the nanofiber (or cardimyocyte) and the nanofiber-collecting electrode. The percentage of aligned cardimyocytes on the aligned NFs is gradually increasing up to 81% approximately to that of the NFs (78.6%, the dashed line) as calculated by ImageJ software in Fig. 4d. The contraction frequency of the uniaxially aligned cell sheet decreases and then maintains at about 1.1 Hz, while the frequency of the random cell sheet is not unique (Fig. 4h).

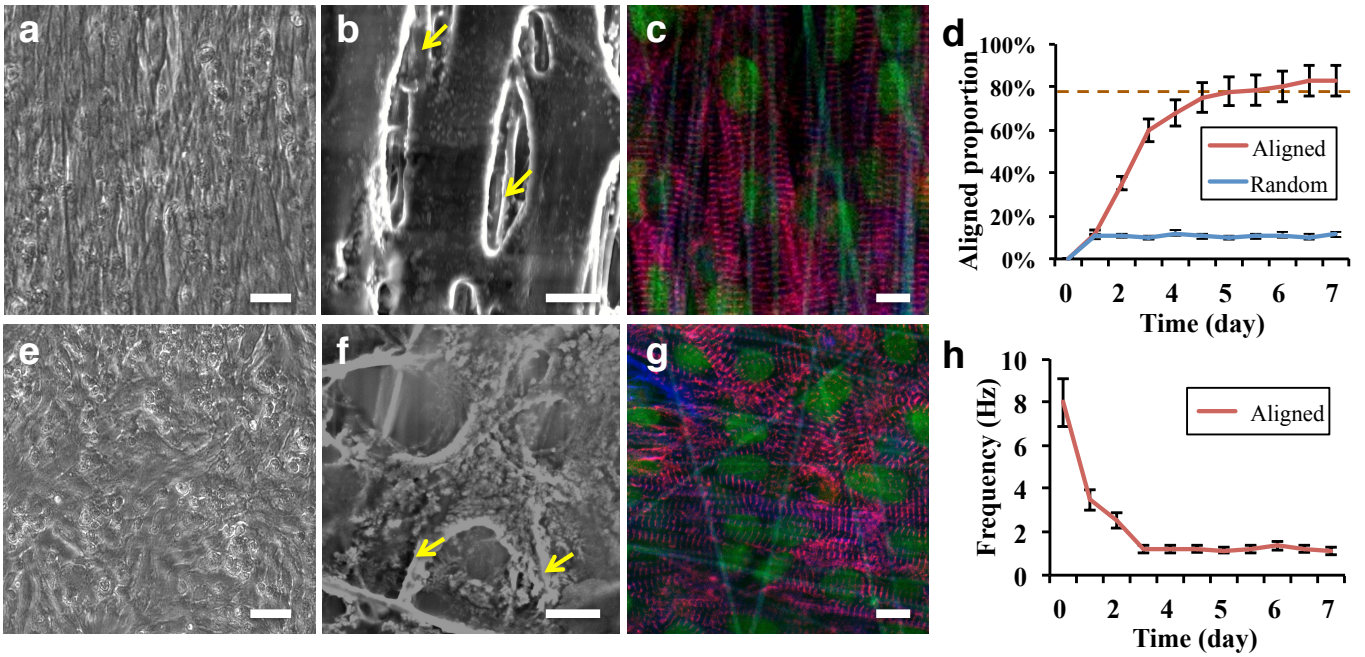

Fig. 4 (**a,e**) The phase-contrast images show uniaxial alignment of the myocardial cell sheet cultured on the uniaxially aligned NFs (a) and no preferential alignment of the myocardial cell sheet cultured on the random NFs (e). (**b,f**) Environmental SEM images of the interface of the single CM and its attached NFs. (b) The NFs guide the CMs to elongate along their directions. (f) There is no obvious relationship between the directions of the cell and the NFs. (The yellow arrows point the NFs.) (**c,g**) Immnofluorescence staining of contractile proteins and nuclei reveals anisotropic (c) and isotropic distribution of CMs (g). (**d**) The percentage of aligned CMs on the aligned NFs is gradually increasing up to 81% approximately to that of the NFs (78.6%, the dashed line). (**h**) The contraction frequency of the uniaxially aligned cell sheet increases and maintains at 1.1 Hz, while the frequency of the random cell sheet is not unique. Scale bar, 50 μm (a,e), 5 μm (others).

Essential mechanodynamic characteristics of original contraction of engineered tissues, like pulse amplitude and frequency, have been investigated.[27,28] Atomic force microscope (AFM) was employed to map the contractile behavior at different regions of a myocardial cell sheet. Until all the cells self-assembled into the confluent cell sheet, a microcantilever gently contacted with an individual cell to allow for simultaneous imaging and patch-clamp recording.[29] The lateral contraction of the cell resulted in the vertical displacement of the membrane. Fig. 5a indicates that the temporal movement of the cell membrane is thereby tracked precisely with the displacement of the microcantilever. The load exerted on the cell sheet was maintained constant at 5 pN while the sheet contracted at a quite steady frequency. We measured the long-time vertical deflections of the five individual CMs that were cell I-V from the screenshot in Fig. 5b (as seen in Movie S1). Cell I contracted periodically at a 1.1 Hz frequency with the vertical deflection coordinating with cell II, III, IV and V (the other four cells around Cell I). Cell II-V had the same characteristics as Cell I, which was defined to construct the contraction mapping of the cell sheet. In contrast from the screenshot in Fig. 5c, Cell I within the random pattern contracted in an unstable period even ceased sometime with vertical deflections varying, as seen as the short-term recording below (Movie S2). In the two cases, the contraction height is both about one hundred and seventy nanometers under the same experimental condition (Fig. 5d,e). The characterization and exploitation of such nonlinear interactions may facilitate the development of more complex biological machines.

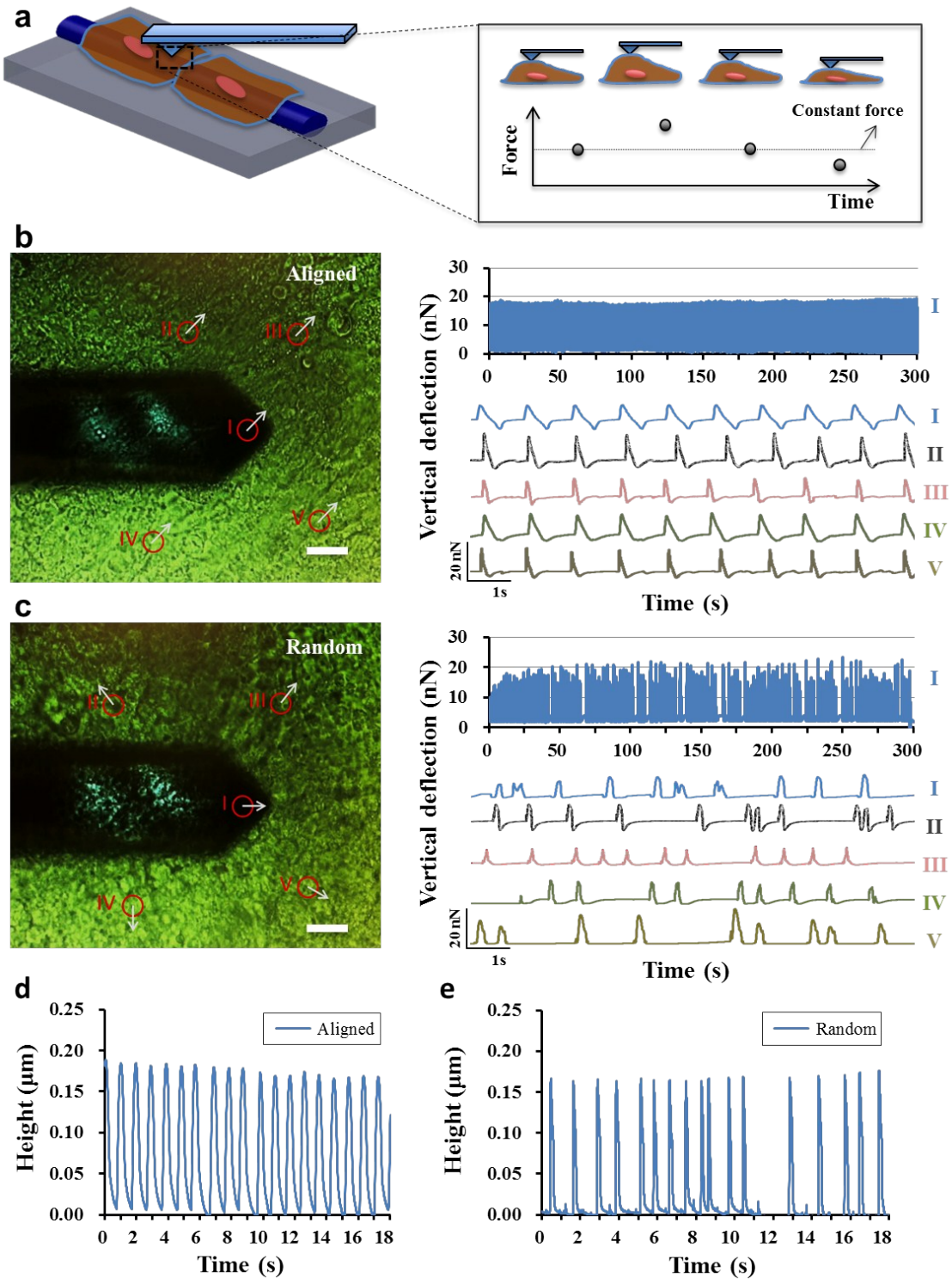

Fig. 5 (**a**) Cartoon illustration shows the operation principle of a microcantilever probing a CM that adheres to the NFs partially embedded in a PDMS film. In the rectangle box, the microcantilever tracks the movement of the cell membrane at a constant load while the CM beats (upper panel). (**b**) An AFM screenshot shows five sites of CMs (red circles) cultured on a uniaxially aligned NF mat. Vertical deflection of site I (the reference cell) was recorded for 5 minutes. Enlarged section of site I (the reference cell) is displayed to show individual beats and periodicity of the contraction, as synchronous as site II, III, IV and V. (The white arrows represent the directions of the CM contraction.) (**c**) An AFM screenshot shows five sites of CMs cultured on a random NF mat. Enlarged section of site I is displayed to show individual beats and instability of the contraction on the mat, as well as site II, III, IV and V. (**d,e**) The contraction height of the CM on the uniaxially aligned (d) and the random NF mat (e). Scale bar, 20 μm.

After five-day cell culture, cooling the biogenerators to room temperature would dissolve the sacrificial PNIPAM layer releasing the biogenerators from the glass cover slip. The biogenerators, termed as bio-bot films, adopted three degrees of freedom during contraction. Synchronously contractile CMs drove the NF mats to bend during systole and return to their original status during diastole. Compared with random pattern, synchronously beating of the CMs on the anisotropic NF mat realized simultaneous contraction and relaxation of the filament along its length, yielding a time-reversible deformation and zero net motion, as observed in Movie S3. During contraction, the aligned bio-bot film buckled to generate a curved shape, with curvature consistent with mechanical considerations for approximately 0.9 second per rotation (Fig. 6a,b). Meanwhile, each contraction of the CMs brought about the bio-bot film to take a fine step forward through the suspending fluid.

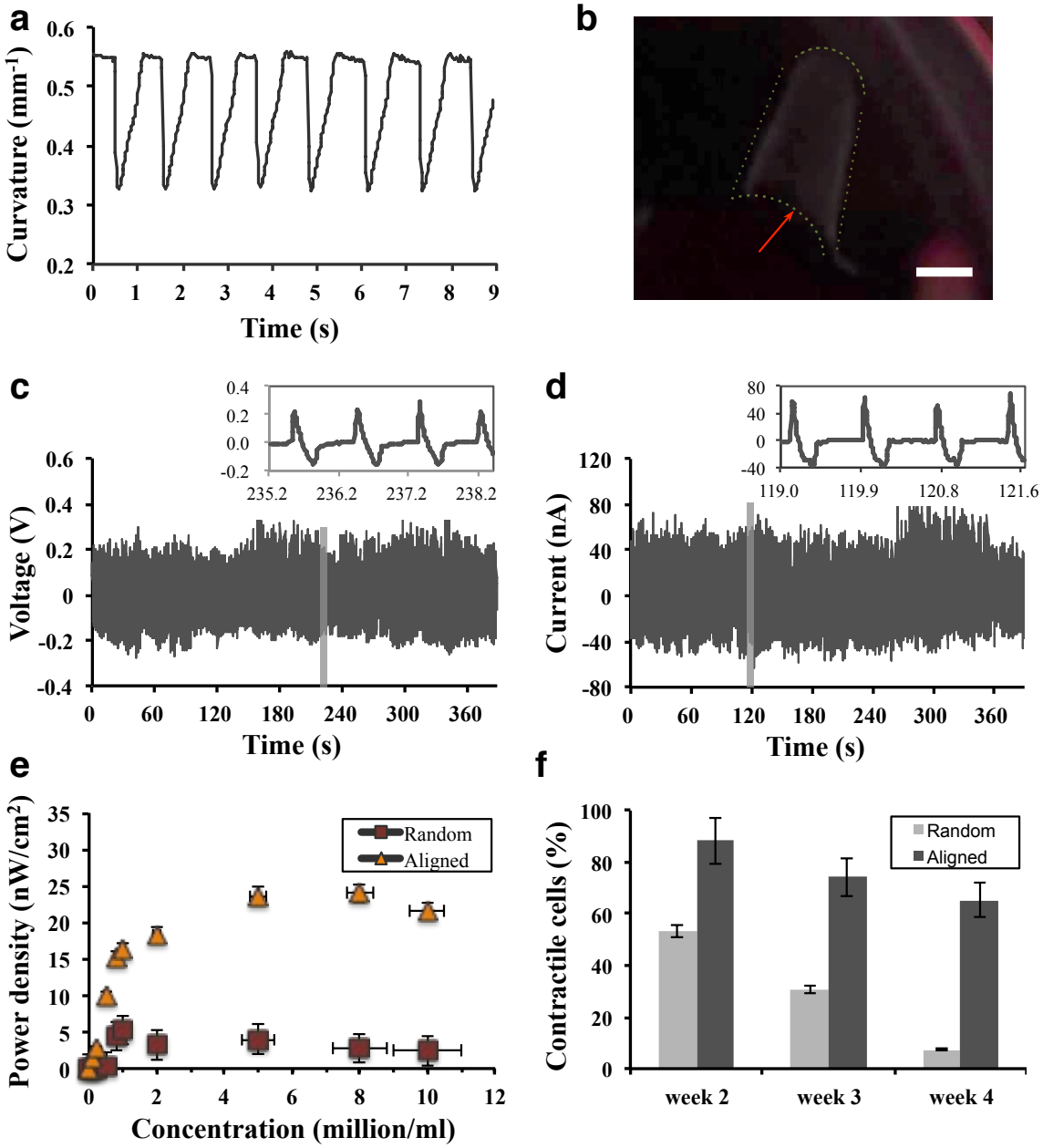

Fig. 6 Bending activation and electrical output of the CCDPN biogenerator. (**a**) The curve shows the curvature of the roll-shaped film based on uniaxially aligned NFs. (**b**) The bio-bot film bends and swims cyclically and locomotively, as observed in Supplementary Movie S3. (**c**) Long-term open-circuit voltage signal and (**d**) short-circuit current signal of the biogenerator based on aligned pattern. The insets show the detailed profiles of the electrical output. (**e**) Dependence of the power density amplitude on the cell concentration. (**f**) The periodic cell viability test is characterized by the property of contractile cells after two-, three-, or four-week cell culture. Scale bar, 5 mm.

Corresponding to the contraction and relaxation of the buckling stress, the aligned bio-bot film bends periodically and generates electrical output when two gold wires are connected with external measurement setup. To begin with, a connection polarity reversion test illuminated that the current and voltage signals were reversed when the biogenerator electrodes were switched, indicating the CCDPN biogenerator produced the measured signals, not from the measuring environment. The aligned biogenerator with the cell concentration of one million/ml achieves 200 mV of average open-circuit voltage and 45 nA of short-circuit current (Fig. 6c,d). Indeed, the cell culture medium may affect the electrical output sort of, but not much as seen in the output periodicity. We also studied the effect of the cell concentration on enhancement of contractile forces of engineered tissues. The electrical output attains the maximum at the eight million/ml concentration and the highest efficiency at the one million/ml concentration on uniaxial NF arrays with the power density of 16.4 nW/cm^2, as shown in Fig. 6e. Since prolonged stability is a major prerequisite for the successful long-term use of the biogenerator, we examined the electrochemical stability of the CCDPN biogenerator *in vitro* for a four-week period. The CCDPN biogenerator remained active throughout the investigation; the percentage of contracting CMs with aligned pattern decreases by 13% during the initial two-week period and is retained at about 68% of the original value for four weeks, while the contractility of random pattern is a lot less than the aligned counterpart (Fig. 6f and Fig. S5). Fig. 6e and 6f were analysed based on the data collected from the signal measurements repeated for six times. These results imply that the biogenerator is thus expected to operate over extended periods with no major deterioration in its performance.

We showed an energy-conversion method that aimed to transfer the nanonewton-ordered biomechanical energy of the CMs to mechanical energy of piezoelectric PVDF NFs. The contraction direction of the CMs was unified by the alignment direction of the NFs; as such the bio-bot film was featured with specific alignment and synchronous contraction. The myocardial cell sheet is a bit thicker than the piezoelectric NF mat and PDMS film, so that the generated strain energy of the piezoelectric NFs could not cancel out, as supported by the result of dependence of power density on PDMS thickness of Fig. S6.[30] The thinner PDMS films have less rigidity to bear myocardial cell sheets and gold wires after releasing. In the case of the PZT fiber generator actuated by tens of layers of random CMs, the output voltage was 40~80 mV.[11] Under the advantage of uniaxial alignment of CMs, couples of layers of cardimyocytes can drive PVDF NFs to bend with 200 mV voltage output. In comparison to thin-film counterparts,[14] the role of piezoelectric PVDF NFs is threefold. First, high-voltage stretching of high crystallinity PVDF NFs by electrospinning technique exhibits a great advantage for scaling up at a low cost and the semi-cured method for collecting NFs allows for non-transfering process. Second, the fused junctions between the biogenerator electrodes and the NFs cause low resistance, also with stable structure when exposing to the cell culture medium. Third, the force/stress required to induce the deformation of the NFs is rather small in comparison with that needed to deform a solid thin-film-based energy harvester, thus permitting nanofiber-based biogenerators to operate in scenarios where only small triggering forces are available, such as in biological systems, small pressure fluctuation and even tiny vibration.

Conclusions

In summary, we have successfully demonstrated a contractile cardiomyocytes-driven piezoelectric nanofiber biogenerator, which exhibits quantitative mechanical-to-electrical energy conversion of neonatal cardiomyocytes in a small contraction regime. The self-contraction of those cardiomyocytes along the nanofiber orientation enables synchronous actuation, thereby causing excellent collective response of the piezoelectric nanofibers. The biogenerator is fabricated by passively seeding of dissociated cardiomyocytes on the fibronectin-coated electrospun PVDF nanofibers with uniaxial alignment. The biogenerator device yields the uniaxial alignment at both the nanofiber level and the cellular level, resulting in the current output of 45 nA and the voltage output of 200 mV at 1.1 Hz frequency. Beyond devices, analysis of device deformation during contraction also has potential for studying biomechanics of myocardial sheets as a model for quantitative mechanical-to-electrical energy conversion. The study thus provides a foundation for a new class of self-propelled bio-bot and biogeneration machines, with reliable microfabrication techniques and application opportunities into *in vivo* biomechanical energy harvesting and human motion monitoring.

Supporting information

The supporting information includes the supplementary methods and figures, and videos of cell contraction and biogenerator bending. The material can be found in the online version.

Acknowledgements

This work is supported by grants from the National Natural Science Foundation of China (No. 61474071, 51273106), National Basic Research Program (973 Program, No. 2015CB352100), the State Key Laboratory of Transducer Technology and a fellowship from China Scholarship Council (CSC). The authors would like to thank J. Chu at CTE lab of UC Berkeley, X. Qiu, C. W. Huang, D. Wang, W. Huang, J. Sia, R. D. Sochol and Y. Liu for their assistance and fruitful discussions. The authors also acknowledge Prof. Yan Shi from Tsinghua University for providing the AFM measuring platform.

References

1 R. Yang, Y. Qin, C. Li, G. Zhu, Z. L. Wang, *Nano Letters,* 2009, **9**, 1201–1205.
2 J. Xi, J. J. Schmidt, C. D. Montemagno, *Nature Materials,* 2005, **4**, 180–184.
3 G. T. Hwang, M. Byun, C. K. Jeong, K. J. Lee, *Adv. Healthcare Mater.,* 2015, **4**, 646–658.
4 C. Dagdeviren, B. D. Yang, Y. Su, P. L. Tran, P. Joe, E. Anderson, J. Xia, V. Doraiswamy, B. Dehdashti, X. Feng, B. Lu, R. Poston, Z. Khalpey, R. Ghaffari, Y. Huang, M. J. Slepian, J. A. Rogers, *PNAS,* 2014, **111**, 1927–1932.
5 A. W. Feinberg, A. Feigel, S. S. Shevkoplyas, S. Sheehy, G. M. Whitesides, K. K. Parker, *Science,* 2007, **317**, 1366–1370.
6 S. A. Thompson, C. R. Copeland, D. H. Reich, L. Tung, *Circulation,* 2011, **123**, 2083–2093.
7 J. You, H. Moon, B. Y. Lee, J. Y. Jin, Z. E. Chang, S. Y. Kim, J. Park, Y. Hwang, J. Kim, *Journal of Biomechanics,* 2014, **47**, 400–409.
8 V. Chan, K. Park, M. B. Collens, H. Kong, T. A. Saif, R. Bashir, *Scientific Reports,* 2012, **2**, 857.
9 J. Kim, J. Park, S. Yang, J. Baek, B. Kim, S. H. Lee, E. S. Yoon, K. Chun, S. Park, *Lab Chip,* 2007, **7**, 1504–1508.
10 J. C. Nawroth, H. Lee, A. W. Feinberg, C. M. Ripplinger, M. L. McCain, A. Grosberg, J. O. Dabiri, K. K. Parker, *Nature Biotechnology,* 2012, **30**, 792–797.
11 T. Ishisaka, H. Sato, Y. Akiyama, Y. Furukawa, K. Morishima, *Solid-State Sensors, Actuators and Microsystems Conference (Transducers 2007),* 903–906.
12 T. Ishisaka, H. Sato, Y. Akiyama, Y. Furukawa, K. Morishima, *28th Annual Int. Conf. IEEE EMBS.*, 2006, 6685.
13 E. Choi, S. Q. Lee, T. Y. Kim, H. K. Chang, K. J. Lee, J. Park, *Sensors and Actuators B,* 2010, **151**, 291–296.
14 X. Liu, X. Wang, S. Li, L. Lin, *Micro Electro Mechanical Systems (MEMS 2014)*, 159–162.
15 X. Wang, J. Liu, J. Song, Z. L. Wang, *Nano Letters,* 2007, **7**, 2475–2479.
16 B. J. Hansen, Y. Liu, R. Yang, Z. L. Wang, *ACS Nano,* 2010, **4**, 3647–3652.
17 H. Chen, C. Jia, C. Zhang, Z. Wang, C. Liu, *IEEE International Symposium on Circuits and Systems (ISCAS 2007)*, 557–560.
18 Z. L. Wang, W. Wu, *Angew. Chem. Int. Ed.,* 2012, **51**, 11700–11721.
19 J. Fang, H. Niu, H. Wang, X. Wang, T. Lin, *Energy Environ. Sci.,* 2013, **6**, 2196–2202.
20 C. Chang, V. H. Tran, J. Wang, Y. K. Fuh, L. Lin, *Nano Lett.,* 2010, **10**, 726–731.
21 J. Chang, M. Dommer, C. Chang, L. Lin, *Nano energy,* 2012, **1**, 356–371.
22 K. K. Parker, J. Tan, C. S. Chen, L. Tung, *Circ Res.,* 2008, **103**, 340–342.
23 C. Cvetkovic, R. Raman, V. Chan, B. J. Williams, M. Tolish, P. Bajaj, M. S. Sakar, H. H. Asada, M. T. A. Saif, R. Bashir, *PNAS,* 2014, **111**, 10125–10130.
24 S. Wong, W. H. Guo, Y. L. Wang, *PNAS,* 2014, **111**, 17176 – 17181.
25 M. L. McCain, H. Lee, Y. A. Schaus, A. G. Kléber, K. K. Parker, *PNAS,* 2012, **109**, 9881–9886.
26 V. Chan, J. H. Jeong, P. Bajaj, M. Collens, T. Saif, H. Kong, R. Bashir, *Lab Chip*, 2012, **12**, 88–98.
27 L. W. Ricotti, A. Menciassi, *Biomed. Microdev.,* 2012, **14**, 987–998.
28 A. Grosberg, P. L. Kuo, C. L. Guo, N. A. Geisse, M. A. Bray, W. J. Adams, S. P. Sheehy, K. K. Parker, *PLoS Computational Biology,* 2011, **7**, e1001088.
29 P. W. Alford, A. W. Feinberg, S. P. Sheehy, K. K. Parker, *Biomaterials,* 2010, **31**, 3613–3621.
30 T. T. Yen, T. Hirasawa, P. K. Wright, A. P. Pisano, L. Lin, *J. Micromech. Microeng.,* 2011, **21**, 085037.

